

Triple-stage mass spectrometry unravels the heterogeneity of an endogenous protein complex

Supporting Information

Gili Ben-Nissan^a, Mikhail E. Belov^b, David Morgenstern^c, Yishai Levin^c, Orly Dym^d, Galina Arkind^a, Carni Lipson^a, Alexander A. Makarov^b and Michal Sharon^{a,*}

^aDepartment of Biological Chemistry, Weizmann Institute of Science, Rehovot 7610001, Israel

^bThermo Fisher Scientific, 28199 Bremen, Germany

^cThe Nancy and Stephen Grand Israel National Center for Personalized Medicine, Weizmann Institute of Science, Rehovot 7610001, Israel

^dIsrael Structural Proteomics Center, Weizmann Institute of Science, Rehovot 7610001, Israel

*Corresponding author:

Michal Sharon

Tel: (+972)-8-934-3947

Fax: (+972)-8-934-6010

Email: michal.sharon@weizmann.ac.il

The Supporting Information includes following items:

Page S3	Yeast strains, media and transformation
Page S3-S4	FLAG-affinity purification of FBP1 from yeast
Page S4-S5	MS ³ analysis
Page S5-S6	Data assignment of MS ³ spectra
Page S6	Intact protein LC-MS analysis
Page S6-S7	Standard proteomic analysis
Page S8	Deconvolution of the measured MS ¹ spectra
Page S8	Modeling the structure of FBP1
Page S9	Figure S1. Parameter settings of the linear ion trap enables dissociation regulations.
Page S10	Figure S2. Forevacuum pressure control enables ion transmission optimization.
Page S11	Figure S3. Deconvolution of the measured MS1 spectra.
Page S12	Figure S4. Monomers and dimers are released from FBP1 upon its activation.
Page S13	Figure S5. The extent of mono-phosphorylation on individual FBP1 subunits is dependent on growth conditions.
Page S14-S15	Figure S6. MS3 fragmentation of FBP1 purified from yeast grown in the absence of glucose, or after exposure to heat shock unravels the existence of two different phosphorylation sites.
Page S16-S17	Figure S7. Bottom up proteomic analysis of FBP1 complexes.
Page S18	Table 1. Theoretical masses of the different FBP1 protein species identified in the MS1 and MS2 measurements.
Page S19	References

Yeast strains, media and transformation

In this study, the yeast strain BY4741 (BY4741; MATa his3 Δ 1 leu2 Δ 0 met15 Δ 0 ura3 Δ 0) or was used (generously provided by J. Gerst, Weizmann Institute). For tagging of the C-terminus of FBP1 with a FLAG tag, we used the template plasmid TOPO 3xFLAG KANMX6 vector (generously provided by M. Schuldiner, Weizmann Institute). The FLAG sequence, encoding the 8 amino acids DYKDDDDK was placed on a forward primer immediately after the last 50 nucleotides of the 3' end of the FBP1 gene. A reverse primer harboring 50 nucleotides complementary to the 3' untranslated region of the FBP1 gene, immediately after the stop codon, was designed to include an adjunct KANMX6 resistance marker. The amplified PCR product was transformed into yeast by standard techniques using LiAcetate/TE/Polyethylene glycol solutions¹, and clones resistant to G418 were isolated and verified by PCR and western blot for FBP1-FLAG expression, using an anti-FLAG antibody. Genomic sequence analysis showed that the endogenous FBP1 gene was correctly tagged with one copy of the FLAG sequence.

For FBP1 expression induction, a single yeast colony was grown overnight in 10 ml YPD [1% (w/v) yeast extract, 2% (w/v) Bacto peptone, 2% (w/v) glucose], at 30 °C. The culture was then diluted 1:20 into the same medium, and grown for additional 5 hours at 30 °C. Cells were then concentrated (500 x g, 5 minutes), dissolved in 700 ml YP medium [1% (w/v) yeast extract, 2% (w/v) Bacto peptone] and grown for 18 hours at 30 °C. For heat shock, cells were moved for 1 hour to 37 °C before harvesting. For growth in glucose, cells were concentrated as before, resuspended in YPD and incubated for 10 minutes at 30 °C before harvesting. Cells were then harvested (5,000 x g, 5 minutes) and the yeast pellets were frozen in liquid nitrogen and stored at -80 °C.

FLAG-affinity purification of FBP1 from yeast

Yeast pellets were thawed in 100 ml lysis buffer [20 mM Tris pH 7.4, 150 mM NaCl, 1% NP-40, protease inhibitors (1 mM PMSF, 1 mM benzamidine, 1.4 μ g/ml pepstatin A), and phosphatase inhibitors (1 mM Na-ortho-vanadate, 1 mM β -glycerophosphate and 2.5 mM Na-pyrophosphate)]. Cells were lysed using a bead-beater (BioSpec) cooled on dry ice in glycerol, using glass beads (425-600 μ m, Sigma)]. Seven consecutive cycles of 1 minute beating, followed by 2-5 minute cooling time, were applied for efficient lysis. Following lysis, samples were centrifuged (14,000 x g, 20 minutes) and the cleared lysate was loaded onto 1 ml of ANTI-FLAG M2 Affinity Gel (Sigma), pre-equilibrated with lysis buffer. The

lysate was incubated with the affinity gel for 3 hours at 4 °C with gentle shaking, and then the gel was drained and washed with 10 ml lysis buffer, 10 ml of wash buffer (50 mM Tris pH 7.4, 150 mM NaCl) and then 20 ml of 0.5 M ammonium acetate. Elution from the affinity gel was done by addition of 4 ml of 0.5 M ammonium acetate containing 0.5 mg/ml FLAG peptide (DYKDDDDK) (GL Biochem). The eluted sample was concentrated to 100 µl, using Amicon ultra-centrifugal filter units with a 30 kDa cut off (Merck). The protein was then aliquoted, snap-frozen in liquid nitrogen and stored at -80 °C.

MS³ analysis

3 µl purified FBP1 was mixed with DMSO and EGTA, to a final concentration of 12.5 % and 125 µM, respectively. The sample was loaded into a gold-coated nano-ESI capillary prepared in-house, as previously described² and sprayed into the mass spectrometers. General instrument parameters used were the following: argon was used as the collision gas in the HCD cell, nanoESI emitter voltage was 1.7 kV and inlet capillary temperature was 180 °C. The capillary temperature value was set after screening for an optimized temperature that on one hand will maintain the protein complexes in their intact native state, while on the other hand provide improved desolvation of the ions. In MS¹ analysis, the linear ion trap was set to the transmission mode, i.e., inject flatapole bias and inter-flatapole lens were maintained at a static voltage of 2 V. Throughout all experiments, the linear ion trap was operated at an RF amplitude of 500 Vpp and an RF frequency of 500 kHz. Bent flatapole DC bias and axial gradient were set to 2 V and 30 V, respectively. To further facilitate desolvation of intact protein complexes, HCD cell bias was dynamically switched to -200 V during an ion injection event at a trapping gas pressure setting of 3, which corresponds to HV pressure of 1.7×10^{-4} mbar and UHV pressure of 5.96×10^{-10} mbar. The HCD multipole was operated at an RF amplitude and standard RF frequency of 900 Vpp and 2780 kHz, respectively. Mass spectra were recorded at a resolving power of 17,500. In the MS² analysis (or, more accurately, pseudo-MS² analysis due to the absence of any mass selection at that step), the linear ion trap was operated in the “trap-and-release” mode, characterized by multiple repeats of trapping and release events³. Each trapping event had a user-defined duration, typically within a range of 2 ms to 20 ms, followed by a 200 µs release event. The sequences of trap and release events were synchronized with an Orbitrap trigger generated by a pulser board. During the trapping event, flatapole bias and interflatapole lens voltage were maintained at -220 V and 10 V, respectively, which resulted in higher-energy collisional activation of the

precursor protein complexes followed by trapping and collisional relaxation of the ejected subunits. During the 200 μ s release events, inject flatapole bias and interflatapole lens voltages were rapidly switched (1 μ s rise time pulses) to 10 V and 2 V, respectively, to ensure efficient purging of the ejected subunits out of the linear ion trap into the bent flatapole. Bent flatapole DC bias and gradient were set to 1.8 V and 15 V, respectively. A rapid increase in the full energy of the trapped complexes / subunits during the release event resulted in auxiliary collision activation and controllable fragmentation of the precursors in the bent flatapole device positioned immediately downstream of the linear ion trap. Unlike in MS¹ experiments, HCD cell bias during an ion injection event was reduced to -10 V at trapping gas pressure setting of 1, which corresponds to HV pressure of 6.3×10^{-5} mbar and UHV pressure of 3.25×10^{-10} mbar. The reduced pressure in the Orbitrap analyzer enabled detection of the ejected subunits, whose signals could not otherwise be acquired at higher pressure due to their faster dephasing rates. In MS³ analysis, the most intense charge state ions were mass-selected using an isolation window of ± 5 Th. For ion isolation we used a standard segmented quadrupole mass filter from a Q Exactive Plus instrument with a modified electronic board that featured decreased resonance frequency of 278 kHz and an upper mass-selection limit above 20000 m/z as described in⁴. Most of the instrument parameters were kept similar to those used in MS² experiments with some exceptions. Specifically, the resolving power was increased up to 140,000, HCD collision energy in the laboratory frame of reference was set between 70 V and 110 V per elementary charge, and the Central Electrode Inject voltage was changed from -3,200 V (used in MS¹ and MS²) to -3,800 V. Mass spectra were averaged for several minutes followed by manual data analysis. The mass spectrometer was externally mass-calibrated using a Cesium Iodide solution at a concentration of 2 mg/ml. No smoothing was applied to any spectra.

Data assignment of MS³ spectra

Theoretical m/z values for the potential fragments of FBP1 were generated using the free online MS-Product software, from the ProteinProspector Tools suite, version 5.18.1 (<http://prospector.ucsf.edu/prospector/cgi-bin/msform.cgi?form=msproduct>). MS¹ and MS² analyses revealed that FBP1 is missing the first Met, therefore, theoretical m/z values were calculated for all possible b^{+1} and y^{+1} ions that can originate from ²Pro – ³⁵⁵Lys, either with or without phosphorylation. A second mass list was generated for the theoretical m/z values of ions resulting from fragmentation of the protein, lacking ²Pro. Raw MS³ files were processed by the Thermo Scientific Xcalibur 3.1.66.10 package, using the Xtract algorithm for

extracting monoisotopic values. These values were compared against the theoretical masses described above and fragments, having a mass accuracy of up to 10 ppm were considered as confident. For each protein sample, the top-down fragmentation results reflect the cumulative data obtained from 2-3 spectra, acquired at different HCD energies.

MS measurements using the Synapt G2 instrument

For CID and SID experiments, analysis was performed on a Synapt G2 instrument (Waters, USA), with a customized SID device installed upstream of the ion mobility separator⁵. The carbon-starved FBP1 sample in 0.5 M ammonium acetate was used. For CID experiments, the voltages on the SID device were set for full transmission of the ions. The following experimental parameters were used: capillary voltage 1.5 kV, sampling cone voltage 100 V, and extraction cone voltage 10 V. A single charge state of 6,572 m/z was isolated and subjected to CID, using trap collision energy of 80 V. Nitrogen was used as the collision gas. For SID experiments, the isolated charge state was collided with the gold-coated surface at acceleration voltage of 40 V. All spectra were calibrated externally by means of a cesium iodide solution (50 mg/ml). Spectra are shown with minimal smoothing, and without background subtraction.

Intact protein LC-MS analysis

LC-MS separation of intact proteins using a monolithic column was performed as previously described⁶. In brief, 5 µl of FBP1 was loaded onto a monolithic column, heated to 60 °C, and eluted over a gradient of 30 – 50 % acetonitrile, during 15 minutes. The FBP1 monomers eluted after 10 minutes and were directly sprayed into a QSTAR XL mass spectrometer (Applied Biosystems, USA), for accurate mass determination.

Standard proteomic analysis

Proteins were denatured using 8 M urea (Sigma, U5128) 0.1 M Tris-HCl, pH 7.9 on ice for 10 minutes. Proteins were then reduced by incubation with 5 mM dithiothreitol (Sigma) for 1 hour at room temperature, and alkylated with 10 mM iodoacetamide (Sigma) in the dark for 45 minutes. Samples were then diluted to 2 M urea with 50 mM ammonium bicarbonate followed by digestion with trypsin (Promega, Madison, WI, USA) overnight at 37 °C (50 : 1 protein amount : trypsin). The digestions were stopped by 1% trifluoroacetic acid. Peptides were desalted using solid-phase extraction columns (Oasis HLB, Waters, Milford, MA, USA)

and stored in -80 °C until further analysis. For liquid chromatography, ULC/MS grade solvents were used in all steps. Each sample was loaded using split-less nano-Ultra Performance Liquid Chromatography (nanoUPLC) (10 kpsi nanoAcquity; Waters, Milford, MA, USA). The mobile phase was: A) H₂O + 0.1% formic acid and B) acetonitrile + 0.1 % formic acid. Desalting of the samples was performed online using a reversed-phase C₁₈ trapping column (180 µm internal diameter, 20 mm length, 5 µm particle size; Waters). Peptides were separated using a HSS T3 nano-column (75 µm internal diameter, 250 mm length, 1.8 µm particle size; Waters) at 0.35 µl/minute. Peptides were eluted from the column into the mass spectrometer using the following gradient: 4% to 30 % B in 105 minutes, 30 % to 90 % B in 5 minutes, maintained at 90 % for 5 minutes and then back to initial conditions. The nanoUPLC was coupled online through a nanoESI emitter (10 µm tip; New Objective, Woburn, MA, USA) to a quadrupole Orbitrap mass spectrometer (Q Exactive Plus, Thermo Fisher Scientific, Bremen, Germany) using a FlexIon nanospray apparatus (Proxeon). Data were acquired in Data Dependent Acquisition mode, using the Top20 method. MS¹ resolution was set to 70,000 (at 400 m/z), maximum injection time was set to 20 milliseconds, AGC target 3e6, mass range 300-1650 m/z. MS² resolution was set to 17,500, quadrupole isolation was set to 1.7 m/z, maximum injection time of 60 milliseconds, dynamic exclusion of 60 seconds and charges 1 and >8 were excluded. For data processing, raw data was imported into Expressionist software (Genedata) version 10. The software was used for retention time alignment, using a pairwise alignment tree, and peak detection of precursor peptides, as described previously⁷. A master peak list was generated from all MS/MS events and sent for database searching using Mascot v2.5.1 software (Matrix Sciences). Data were searched against the *Saccharomyces cerevisiae* sequences in UniprotKB, version 2016_02, appended with common laboratory contaminant proteins. Fixed modification was set to carbamidomethylation of C and variable modification was set to oxidation of M, deamidation of N or Q and phosphorylation of S, T or Y. Error tolerance for MS¹ was set to 10 ppm and 20 ppm for MS². Search results were then filtered using the PeptideProphet algorithm⁸, embedded into Scaffold software version 3.7 using a (Proteomesoftware), to achieve maximum false discovery rate of 1% at the protein level. Peptide identifications were imported back to the Expressionist software to annotate identified peaks. Quantification was based on the maximum height of the extracted ion chromatograms from Expressionist.

Deconvolution of the measured MS¹ spectra

Deconvolution was performed for each MS¹ spectra using the peakfit v4 software (Jandel Scientific, San Rafael, CA). In this program, peaks are fitted automatically to a series of Gaussians using a deconvolution approach. A numerical fitting procedure was repeated to minimize the deviation from experimental data as monitored by the coefficient of determination, R².

Modeling the structure of FBP1

The FBP1 is homologous to the Fructose-1,6-bisphosphatase from *Sus sacrofa* (PDB code 1NUW with 48% sequence identity). Based on this structure, the full-length sequence of the yeast FBP1 protein was entered into the web interface of Protein Homology/analogy Recognition Engine Phyre2 portal⁹, for modeling the structures of this protein. A preliminary 3D structural model was obtained for the protein, spanning from ¹⁸Thr to ³⁴⁷Ser, which accounts for 92% of the sequence, with 100% confidence. The FBP1 tetramer was generated using crystallographic symmetry elements in the I222 space group of the 1NUW structure.

Supplementary Figures

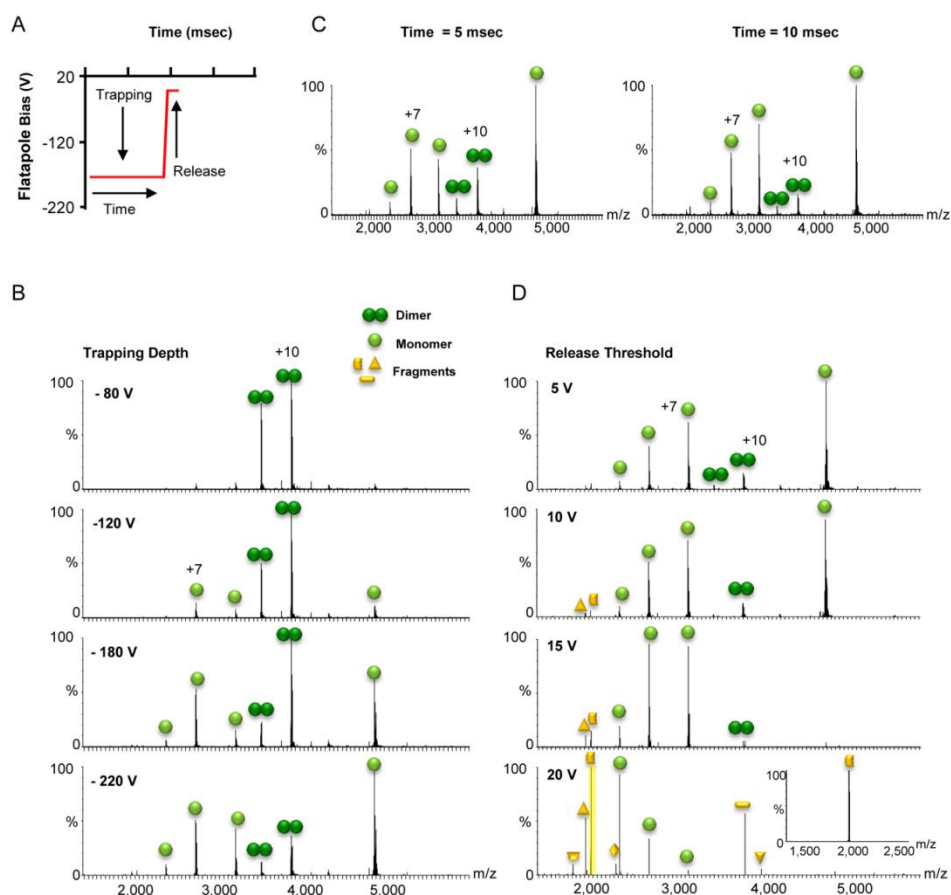


Figure S1. Parameter settings of the linear ion trap enables dissociation regulations. (A) Schematic representation of the main linear ion trap parameters that affect dissociation; i.e., the trapping well depth (V), trap and release times (ms) and linear ion trap activation bias during the release event (V). (B) The homodimeric model protein DJ-1 was subjected to progressive deepening (from -80 V and up to -220 V) of the trapping well, inducing dimer dissociation into monomers. (C) Extending the trapping time in the linear ion trap enhances dissociation. (D) Elevation of the linear ion trap activation bias from 5 V to 20 V during the release event resulted in additional activation of the ejected subunits, and led to partial fragmentation of the DJ-1 monomer into backbone fragments. The inset within the spectrum acquired at activation bias of 20 V, shows isolation of the 2,124 m/z fragment ion (highlighted in yellow), within the quadrupole mass filter (#4 in Fig. 1). This result confirms that backbone fragmentation occurs upon the release from the linear ion trap and not due to fragmentation within the HCD cell (#6 in Fig. 1).

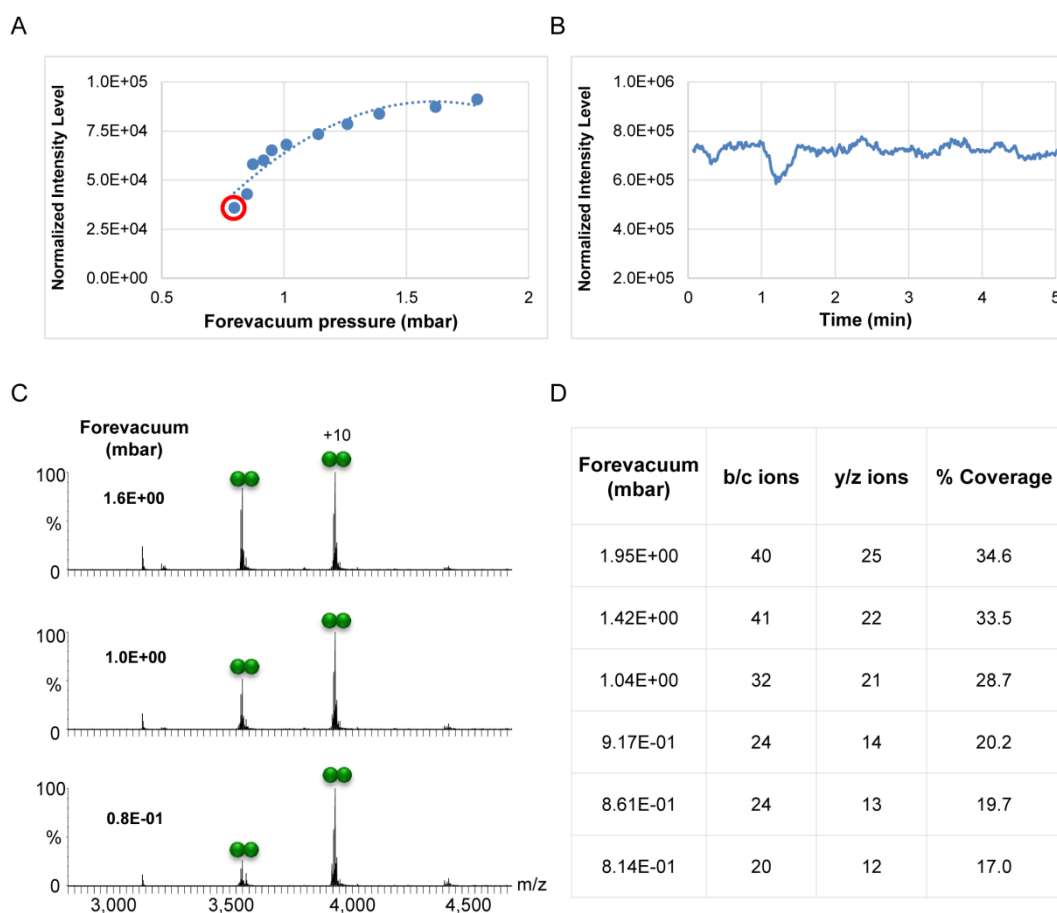


Figure S2. Forevacuum pressure control enables ion transmission optimization. A tunable vacuum pump controlling the forevacuum pressure was installed, and the resulting effect on various experimental values was examined using the model protein DJ-1. (A) Low forevacuum pressure reduces the Normalized Intensity Level, as can be seen by the low signal intensity that is observed in the absence of pressure control (labeled by a red circle). Dashed line represents an order 2 polynomial trendline. (B) Signal intensity, measured at a constant forevacuum pressure (1.44 mbar) is stable over a period of at least 6 minutes. (C) Lower forevacuum pressure causes a bias against higher charge states of the DJ-1 dimer. (D) MS³ efficiency is negatively affected by suboptimal forevacuum pressure, as evaluated by the ProSight software.

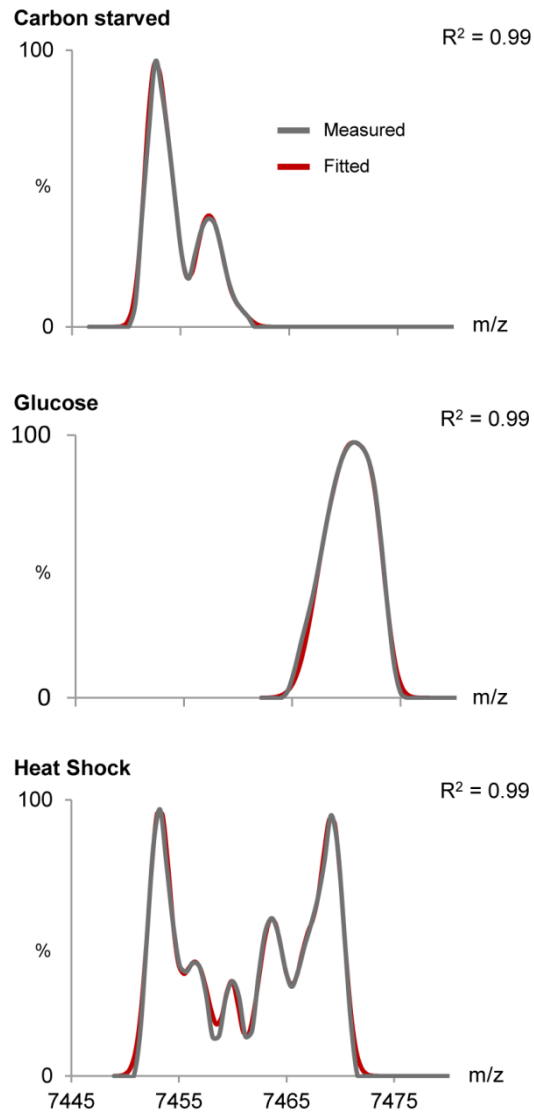


Figure S3. Deconvolution of the measured MS¹ spectra. A close agreement is seen between the deconvoluted data (in red) and the measured MS¹ spectra (in grey), of the FBP1 complexes purified from the different growth conditions. The coefficient of determination value (R^2) of the fits is indicated above each graph.

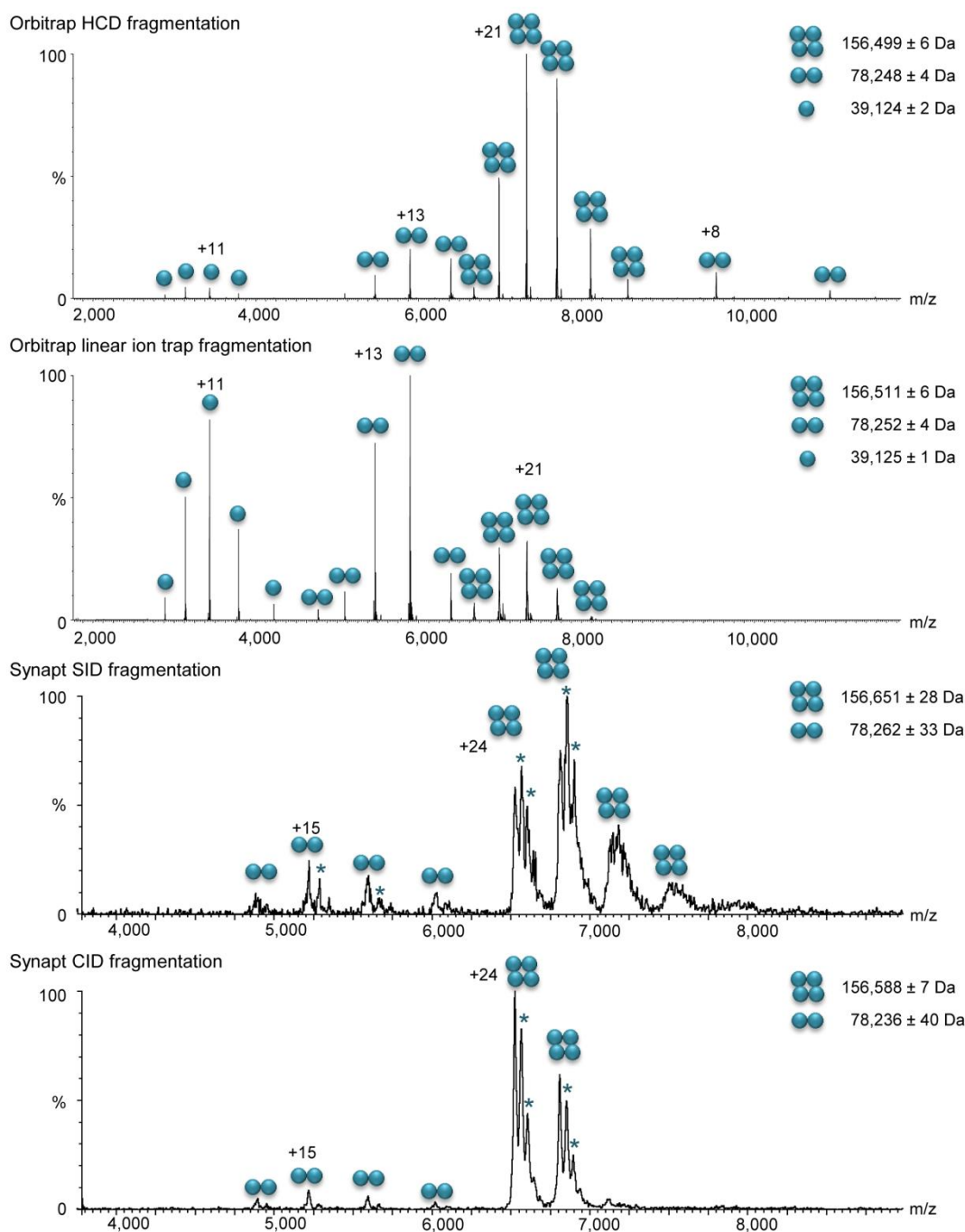


Figure S4. Monomers and dimers are released from FBP1 upon its activation. The FBP1 complex was analyzed on the modified Q Exactive Plus and on the Synapt G2 instruments. The complex was subjected to dissociation either within the HCD or linear ion trap cells of the Orbitrap platform, or by surface induced dissociation (SID) and collision induced dissociation (CID) on the Synapt mass spectrometer. All types of activation resulted in the dissociation of the tetramer into dimers, indicating that the intact assembly is a dimer of two dimers. Orbitrap HCD, and to a higher extent Orbitrap linear ion trap fragmentation, also led to the generation of monomers. Species denoted with asterisks are bound to a FLAG peptide, an adduct remaining from the purification procedure.

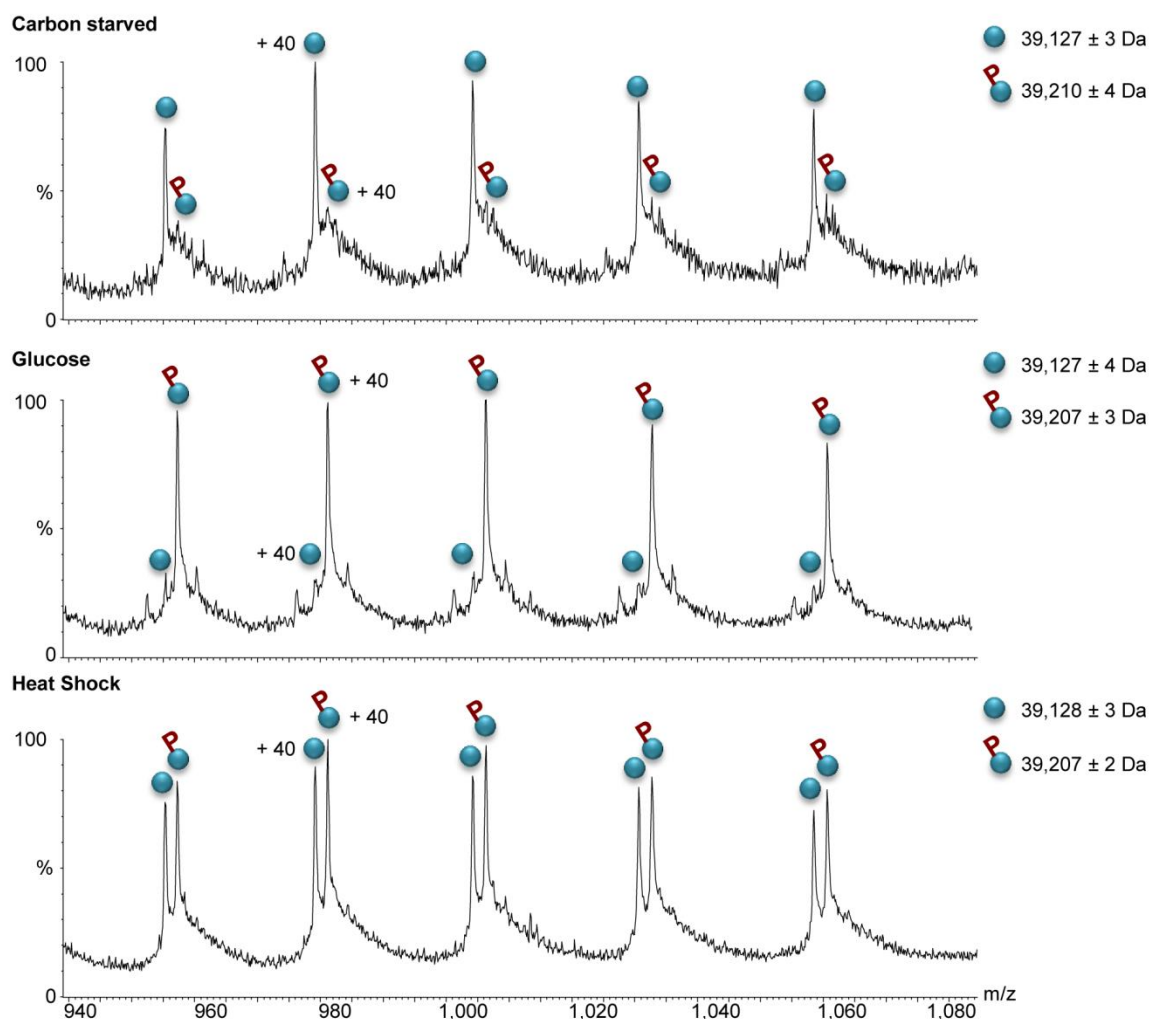


Figure S5. The extent of mono-phosphorylation on individual FBP1 subunits is dependent on growth conditions. FBP1 complexes, purified from yeast grown under different conditions were subjected to LC separation on a monolithic column under denaturing conditions and on-line ESI-QToF MS analysis of intact proteins. The results show that in response to different growth conditions the amount of mono-phosphorylated FBP1 subunits is altered. Overall, when comparing the relative abundance of the unmodified and mono-phosphorylated subunits within the different FBP1 preparations, they are similar to those obtained by the MS² approach (Fig. 3). The somewhat higher abundance of the mono-phosphorylated form of FBP1 after exposure to heat shock, observed here, may be due to the loss of the liable phosphate group during the MS² process. The FBP1 monomers are graphically depicted as blue circles. Phosphorylations are labeled by red “P”.

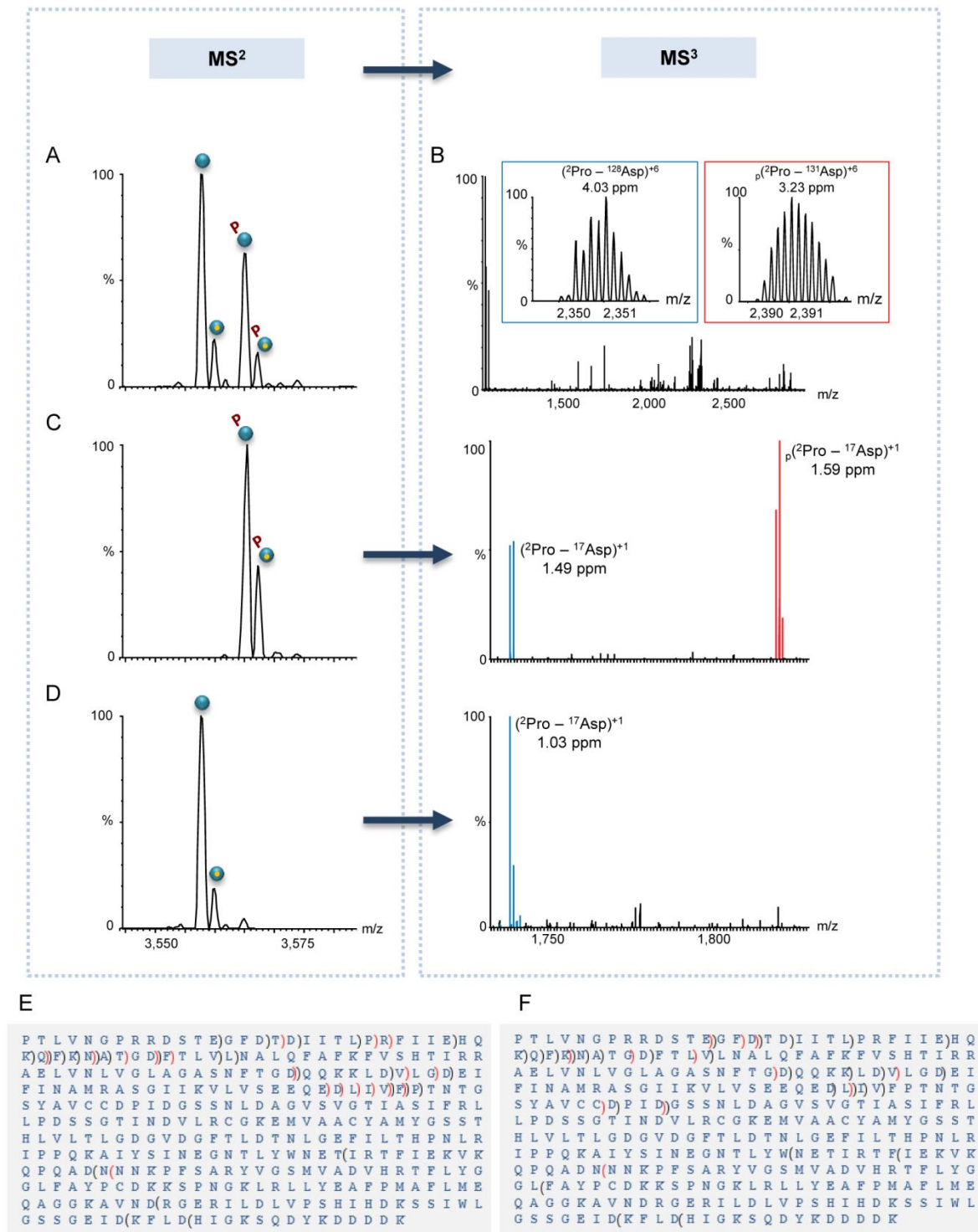


Figure S6. MS³ fragmentation of FBP1 purified from yeast grown in the absence of glucose, or after exposure to heat shock unravels the existence of two different phosphorylation sites. (A-D) Representative spectra of FBP1, purified from yeast exposed to heat shock. MS² isolation of mono-phosphorylated and unmodified FBP1 forms (A) and the corresponding MS³ fragmentation spectrum (B). In all generated MS³ spectra, fully resolved multiply charged fragment ions were detected using a mass resolution of 140,000. For each fragment, the position, as well as the charge and mass accuracy are indicated. The

insets show fragment ion matches of two *b* ions, representing unmodified (blue box) and phosphorylated (red box) peptides. Phosphorylated fragments are labeled by _p. (C-D) Selective MS² isolation of mono-phosphorylated or unmodified FBP1 proteoforms. For each proteoform selected, the respective MS³ spectrum is shown on the right panel of (C) or (D). (C) The phosphorylated FBP1 proteoform was selected and subjected to MS³ fragmentation (left panel). Expansion of the 1,700-1,900 m/z region of MS³ data generated (right panel), shows the phosphorylated *b16* ion, which matches the ²PTLVNGPRRDSTEGFD¹⁷ sequence (labeled in red). (D) Selection and fragmentation of the unmodified FBP1 proteoform showed only the non-phosphorylated *b16* ion (labeled in blue). Expansion of the 1,700-1,900 m/z region of MS³ data generated upon specific proteoform selection and fragmentation, showing the *b16* ion, which matches the ²PTLVNGPRRDSTEGFD¹⁷ sequence. The data indicates that the *b16* phosphopeptide is exclusively found in the MS³ spectrum of the mono-phosphorylated FBP1 and not in that of the unmodified proteoform. (E-F) Sequence coverage maps generated for FBP1, purified from yeast grown in the absence of glucose (E), or after exposure to heat shock (F). Identification of the generated peptides indicated the presence of phosphorylation at two mutually exclusive sites: at either position ¹²Ser/¹³Thr or within the stretch of ²⁴⁸Asn-³¹⁰Asp, as shown for FBP1 isolated after shift to glycolysis. Non-phosphorylated fragments are indicated in black, phosphorylated fragments are indicated in red. *b* ions are indicated by brackets pointing towards the N-terminus and *y* ions are indicated by brackets pointing towards the C-terminus.

A

FBP1 sample	Peptide	Site	Probability	Score	Link to raw data
Carbon starved	RD _p S TEGFDTDIITLPR	¹² S	93.94 %	62.7	RDSTEGFDTDIITLPR
		¹³ T	6.05 %	50.8	RDSTEGFDTDIITLPR
		¹⁸ T	0.01 %	20.4	RDSTEGFDTDIITLPR
	DS _p T EGFDTDIITLPR	¹³ T	95.82 %	117.3	DSTEGFDTDIITLPR
		¹² S	4.18 %	103.7	DSTEGFDTDIITLPR
		¹⁸ T	0.00 %	41.9	DSTEGFDTDIITLPR
	TFLYGGFLFA _p Y PCDK	²⁷⁰ Y	0.00 %	4.6	TFLYGGFLFAYPCDKK
		²⁷⁶ Y	100.00 %	52.9	TFLYGGFLFAYPCDKK
Glucose	RD _p S TEGFDTDIITLPR	¹² S	97.15 %	84.6	RDSTEGFDTDIITLPR
		¹³ T	2.85 %	69.3	RDSTEGFDTDIITLPR
		¹⁸ T	0.00 %	37	RDSTEGFDTDIITLPR
	DS _p T EGFDTDIITLPR	¹³ T	49.99 %	61.2	RDSTEGFDTDIITLPR
		¹² S	49.99 %	61.2	RDSTEGFDTDIITLPR
		¹⁸ T	0.01 %	24.4	RDSTEGFDTDIITLPR
	TFLYGGFLFA _p Y PCDK	²⁷⁶ Y	100.00 %	88.4	TFLYGGFLFAYPCDK
		²⁷⁰ Y	0.00 %	8.1	TFLYGGFLFAYPCDK
Heat shock	RD _p S TEGFDTDIITLPR	¹² S	97.96 %	84.7	RDSTEGFDTDIITLPR
		¹³ T	2.04 %	67.8	RDSTEGFDTDIITLPR
		¹⁸ T	0.00 %	39.7	RDSTEGFDTDIITLPR
	DS _p T EGFDTDIITLPR	¹³ T	49.99 %	64.4	RDSTEGFDTDIITLPR
		¹² S	49.99 %	64.4	RDSTEGFDTDIITLPR
		¹⁸ T	0.02 %	29.6	RDSTEGFDTDIITLPR

B

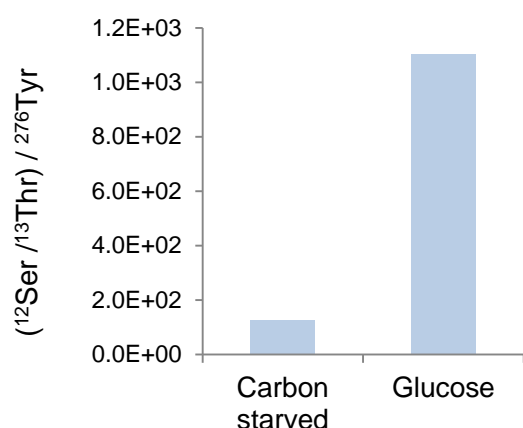






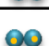

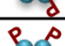
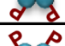
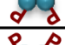








Figure S7. Bottom up proteomic analysis of FBP1 complexes. Bottom up proteomic analysis identified three phosphorylation sites in the carbon starved and glucose samples, at ¹²Ser, ¹³Thr and ²⁷⁶Tyr. (A) The table lists the identified phosphopeptides, their sequence, phosphorylation site, score and localization probability, as calculated by the Mascot software.

In the heat shock sample, phosphorylation was identified at the $^{12}\text{Ser}/^{13}\text{Thr}$ site, however, manual inspection of the data showed that the reported intensity for a potential ^{276}Tyr phosphopeptide was essentially background noise. (B) The fold change of the phosphopeptide intensities in the MS^1 spectra of the carbon starved and glucose samples were summed and ratio of $^{12}\text{Ser}/^{13}\text{Thr}$ to ^{276}Tyr phosphorylation in each sample was calculated, as shown in the bottom bar graph. It can be seen that there was a significant shift towards $^{12}\text{Ser}/^{13}\text{Thr}$ versus ^{276}Tyr phosphorylation in the glucose treatment compared to the carbon starved sample.

Table 1. Theoretical masses of the different FBP1 protein species identified in the MS¹ and MS² measurements.

Protein Species ^a	Theoretical Mass (Da) ^b
	156,505
	156,530
	156,610
	156,634
	156,658
	156,714
	156,578
	156,770
	156,825
	156,874
	156,922

Protein Species	Theoretical Mass (Da)
	39,126
	39,151
	39,206
	39,231
	39,255
	39,175

^aEach FBP1 subunit is graphically depicted as cyan circle. Mg²⁺ ions are indicated as small orange circles, and phosphorylations are labeled as “P”.

^bMasses were calculated according to the protein sequence of the FLAG-tagged FBP1, after removal of the N-terminal methionine.

References

1. Gietz, D.; St Jean, A.; Woods, R. A.; Schiestl, R. H., *Nucleic acids research* **1992**, *20*, 1425.
2. Kirshenbaum, N.; Michaelievski, I.; Sharon, M., *Journal of visualized experiments : JoVE* **2010**.
3. Belov, M., *US Patent* **2014**, 2015/0340213 A1.
4. Belov, M. E.; Damoc, E.; Denisov, E.; Compton, P. D.; Horning, S.; Makarov, A. A.; Kelleher, N. L., *Analytical chemistry* **2013**, *85*, 11163-11173.
5. Zhou, M.; Huang, C.; Wysocki, V. H., *Analytical chemistry* **2012**, *84*, 6016-6023.
6. Rozen, S.; Tieri, A.; Ridner, G.; Stark, A. K.; Schmalzer, T.; Ben-Nissan, G.; Dubiel, W.; Sharon, M., *Methods* **2013**, *59*, 270-277.
7. Shalit, T.; Elinger, D.; Savidor, A.; Gabashvili, A.; Levin, Y., *Journal of proteome research* **2015**, *14*, 1979-1986.
8. Keller, A.; Nesvizhskii, A. I.; Kolker, E.; Aebersold, R., *Analytical chemistry* **2002**, *74*, 5383-5392.
9. Kelley, L. A.; Mezulis, S.; Yates, C. M.; Wass, M. N.; Sternberg, M. J., *Nature protocols* **2015**, *10*, 845-858.